

# RSC Advances



This is an *Accepted Manuscript*, which has been through the Royal Society of Chemistry peer review process and has been accepted for publication.

*Accepted Manuscripts* are published online shortly after acceptance, before technical editing, formatting and proof reading. Using this free service, authors can make their results available to the community, in citable form, before we publish the edited article. This *Accepted Manuscript* will be replaced by the edited, formatted and paginated article as soon as this is available.

You can find more information about *Accepted Manuscripts* in the [Information for Authors](#).

Please note that technical editing may introduce minor changes to the text and/or graphics, which may alter content. The journal's standard [Terms & Conditions](#) and the [Ethical guidelines](#) still apply. In no event shall the Royal Society of Chemistry be held responsible for any errors or omissions in this *Accepted Manuscript* or any consequences arising from the use of any information it contains.

# Controlled inversion and surface disorder in zinc ferrite nanocrystallites and their effects on magnetic properties

Ranajit Sai,\*<sup>a</sup> Suresh D. Kulkarni,<sup>a,b</sup> Swetha S. M. Bhat,<sup>c</sup> Nalini G. Sundaram,<sup>c</sup> Navakanta Bhat<sup>a</sup> and S. A. Shivashankar\*<sup>a</sup>

<sup>a</sup>Centre for Nano Science and Engineering, Indian Institute of Science, Bangalore-560012, India, Fax: 9-80-2360-4656;  
Tel: 91-80-2293-3323; E-mail: ranajit.sai@gmail.com, shivu@cense.iisc.ernet.in

<sup>b</sup>Centre for Atomic and Molecular Physics, Manipal University, Manipal-576104, India

<sup>c</sup>Materials Science Division, Poornaprajna Institute of Scientific Research, Bangalore-560080, India

## Abstract:

A new strategy to control the inversion of zinc ferrite nanocrystallites is demonstrated, while the correlation of process-structure-property is understood with the help of thorough structural and magnetic characterization. It is found that a very high degree of inversion (>0.5) could be induced by rapid microwave-assisted synthesis carried out below 100 °C. Rietveld refinement of high resolution X-ray diffraction patterns of various annealed samples has been employed to investigate the influence of the nature of post-synthesis annealing and the temperature of annealing on the degree of inversion. It is found that magnetization follows the degree of inversion more closely than it does the size of the nanocrystals. Furthermore, slow and prolonged (2 hrs.) annealing results in very different magnetic characteristic than short pulse (2 min) thermal treatment does. Temperature-dependent magnetization (M-T plots) studies confirmed the superparamagnetic nature of all annealed samples which displayed relatively high blocking temperatures (25 K to 56 K) than bulk zinc ferrite (10 K). Coercivity follows the trend of blocking temperature closely. Samples subjected to rapid annealing are found to be associated with a degree of surface disorder that influences the coercivity profoundly. Magnetic measurements suggest that rapid annealing can effectively control the surface disorder in zinc ferrite nanocrystallites, which can screen the interparticle dipolar interaction and thus coercivity. Therefore, a combination of microwave-assisted synthesis to induce a high degree of inversion, followed by different annealing protocols to tune the inversion, can deliver magnetic ferrites of desired characteristics to meet futuristic applications.

## Introduction:

The study of magnetic interactions in spinel ferrite nanocrystallites and their processing-structure-property interrelationship is of importance both to achieve a better understanding of magnetic interactions and to pursue a wide variety of applications, ranging from sensors to biomedicine to radio-frequency integrated circuits.<sup>1-9</sup> Ferrites boast a unique combination of magnetic and electric properties (high magnetization and high resistivity), even at the nanoscale. The origin of such properties of spinel ferrites is in their structure, with cations distributed among tetrahedrally coordinated A sites (8 per unit cell) and octahedrally coordinated B sites (16 per unit cell), so that a generic formula of a normal spinel can be written as  $(\text{Me}^{2+})[\text{Fe}^{3+}_2]\text{O}_4$ , with () and [] representing A and B sites, respectively, 'Me' standing for any divalent metal. In general, magnetic characteristics of spinel ferrites are largely governed by three types of antiferromagnetic superexchange (ASE), namely,  $J_{AA}$  (A-O-A),  $J_{AB}$  (A-O-B), and  $J_{BB}$  (B-O-B), between the  $\text{Fe}^{3+}$  and  $\text{Me}^{2+}$  ions on the A and B sites, each mediated by oxygen ions.<sup>10,11</sup> Among them,  $J_{AB} \gg J_{BB}$ , whereas  $J_{AA}$  is small due to the large separation between two A-site ions, forcing an

1 antiparallel alignment of the moments on the A and the B sites. Furthermore, the dominant ASE,  $J_{AB}$ , is very sensitive to Néel  
2 temperature ( $T_N$ ) which, in turn, is heavily influenced by interionic distance (A-O-B) that can be expressed in terms of the  
3 lattice parameter ( $a$ ) and the oxygen parameter ( $u$ ) - a quantitative measure of the displacement of oxygen ions in the spinel  
4 lattice due to any deformation.<sup>12,13</sup> Owing to the difference in the size of cations, any alteration in their distribution changes  
5 the lattice constant and the oxygen parameter, thereby altering spin interactions that determine  $J_{AB}$ . Therefore, the distribution  
6 of cations among the A and B sites is critically important, particularly in the nanometric regime, to the properties of spinel  
7 ferrites ( $MFe_2O_4$ ; M: Mn, Zn, Ni etc.)<sup>14-16</sup> with different nanostructures, including nanotubes,<sup>16</sup> nanowires,<sup>15</sup> apart from  
8 nanocrystalline powder.

9 In particular, the effect of cation distribution in  $ZnFe_2O_4$  is profound due to the presence of non-magnetic zinc ions in the  
10 lattice, leading to ASE which depends solely on the distribution of  $Fe^{3+}$  ions, and has thus engaged many scientists and  
11 technologists over the years. In zinc ferrite, a normal spinel in the bulk, divalent and non-magnetic  $Zn^{2+}$  ions preferentially  
12 occupy the A sites, while all the B sites are occupied by  $Fe^{3+}$  ions, leaving  $J_{BB}$ , the antiferromagnetic interaction, as the  
13 operative one. However, under certain conditions of synthesis, especially at the nanoscale, the distribution of  $Fe^{3+}$  and  $Zn^{2+}$   
14 ions among the A and B sites is altered, leading to a partially inverted spinel structure,  $(Zn^{2+}_{1-x}Fe^{3+}_x)[Zn^{2+}_xFe^{3+}_{2-x}]O_4$  where  
15 'x' is the inversion parameter, and surprising magnetic characteristics. As a result, the study of magnetization in  $ZnFe_2O_4$  can  
16 lead not only to a better understanding of structure-property relationship in spinel ferrites but also, perhaps, to additional  
17 practical applications for them. It is established that the augmentation of inversion is not directly associated with surface  
18 effects caused by the reduction of grain size but with the method of synthesis.<sup>1</sup> Therefore, to induce inversion in  $ZnFe_2O_4$   
19 nanocrystallites, various synthesis techniques, particularly those which operate away from equilibrium, have been adopted,  
20 such as high energy ball-milling,<sup>17,6,18</sup> co-precipitation,<sup>19</sup> hydrothermal,<sup>1,19</sup> reverse micelles,<sup>20,21</sup> and sol-gel processing<sup>22</sup>.  
21 While various degrees of inversion were observed, very little has been said about the practical way of controlling inversion  
22 and surface disorder so as to tune the properties of ferrites. For example, Ehrhardt *et al.*<sup>18</sup> have shown that inversion  
23 parameter 'x' can be increased by increasing the energy of ball-milling. But, such increase in energy of ball-milling also  
24 resulted in the reduction in crystallite size. And Upadhyay *et al.*<sup>19</sup> claimed that degree of inversion depends mostly on  
25 crystallite size rather than on the process of synthesis. On the other hand, Lemine *et al.*<sup>17</sup> suggested that 'x' can be increased  
26 by employing high temperature annealing after ball-milling, in contrast with the finding of Oliver *et al.*<sup>6</sup>, who noticed that 'x'  
27 in ball-milled samples actually decreased with increasing post-mill annealing temperature. Thus, there has been little clarity  
28 and much confusion when methods for controlling the inversion parameter in ferrite nanocrystals are discussed. In recent  
29 years, the microwave-assisted solvothermal technique has attracted a lot of attention as it is a rapid and far-from-equilibrium  
30 in nature and thus can induce a larger degree of inversion in zinc ferrite nanocrystallites than any other soft-chemical  
31 process.<sup>23-27</sup> In our earlier work,<sup>27</sup> we surmised, by observing their exotic magnetic characteristics, the plausible presence of  
32 inversion in zinc ferrite nanocrystallites prepared by such a microwave-assisted technique. We also noted the dependence of  
33 magnetic behaviour on the post-synthesis annealing technique rather than on the temperature of annealing, but the  
34 relationship between processing technique and inversion parameter were not established. Therefore, there is indeed a need for  
35 a better-understood and practical way of tailoring the inversion and thus the magnetic characteristics of spinel ferrites.

36 In this report, a thorough investigation of structural and magnetic characterization of zinc ferrite nanocrystallites prepared by  
37 the microwave-assisted synthesis technique, followed by various anneal protocols, is described. Rietveld refinement of high

1 resolution X-ray diffraction data of the annealed samples brings out the extent of inversion in each sample, enabling its  
 2 correlation with magnetic measurements of those samples. The effect of synthesis process and post-synthesis annealing on  
 3 the degree of inversion and surface disorder is discussed in light of the resulting structural and magnetic data. Finally, based  
 4 on experimental evidence, we propose an alternative strategy to control inversion: to induce a sufficiently high degree of  
 5 inversion during synthesis first, and then to “tune down” the inversion through appropriate post synthesis annealing.

## 6 Experimental:

7 Nanocrystalline  $\text{ZnFe}_2\text{O}_4$  powder was prepared<sup>27</sup> by a microwave irradiation-assisted synthesis technique, from an aqua-  
 8 alcoholic solution comprising stoichiometric quantities of acetylacetonates of Zn (II) and Fe (III). The as-prepared powder  
 9 (UA00) was then annealed, employing four different annealing protocols.<sup>27</sup> Upon annealing the as-prepared sample in air for  
 10 2 hours at 300°C and 500°C in a conventional muffle furnace, samples CA32 and CA52, respectively, were obtained.  
 11 Separately, UA00 was annealed at 300°C and 500°C for two minutes in air in a home-made rapid annealing furnace, resulting  
 12 in samples RA32 and RA52, respectively. Detailed investigation of crystallinity, microstructure, and particle size distribution  
 13 of the aforesaid samples has been reported elsewhere,<sup>27</sup> while the mean size of the crystallites and some basic magnetization  
 14 data are summarized in Table S1 in the supplementary section for further comparison and discussion.

15 For the Rietveld refinement, high-resolution room temperature X-ray diffraction data were collected for all four annealed  
 16 samples on a Bruker D2 Phaser X-ray powder diffractometer (Cu- $K_\alpha$  radiation, nickel filter, reflection mode), equipped with  
 17 a Lynx-eye detector. The X-ray data were gathered in the range  $2\theta = 5$  to  $80^\circ$  at steps of  $0.02^\circ$ , with exposure time of 6 s per  
 18 step. Magnetic measurements on the powder samples were made using a SQUID magnetometer (Quantum Design MPMS  
 19 XL-5) in the temperature range of 5-300 K, under fields up to 5 T. Magnetic measurements were made after cooling the  
 20 samples first to 5 T in zero field (ZFC) and then under an applied field of 50 Oe and 1 T, while heating the samples to room  
 21 temperature. Measurements from 300 – 5 K were made in the field-cooling (FC) mode, also at the fields of 50 Oe and 1 T.  
 22 The results of these structural and magnetic measurements on the various samples are summarized in Table 1.

23 **Table 1: Crystallographic parameters of the annealed samples**

ID	Refined Formula	D ( $\sigma$ )	x	a (in Å)	Bond Length (in Å)		Bond Angle Zn-O-Fe	R (I, hkl)	M <sub>s</sub>	H <sub>c</sub>	T <sub>B</sub>	T <sub>0</sub>
					at 5 K	at 5 K			emug	Oe	K	K
		nm			Fe-O	Zn-O						
CA32	(Zn <sub>0.5</sub> Fe <sub>0.5</sub> ) [Fe <sub>1.5</sub> Zn <sub>0.5</sub> ] O <sub>3.98</sub>	8.5 (1.03)	0.50	8.409	2.06	1.92	123.3°	3.59	48.1	580	38	250
RA32	(Zn <sub>0.5</sub> Fe <sub>0.5</sub> ) [Fe <sub>1.6</sub> Zn <sub>0.4</sub> ] O <sub>4.05</sub>	17.5 (3.25)	0.49	8.423	2.07	1.87	124.2°	3.59	46.6	1020	40	200
CA52	(Zn <sub>0.8</sub> Fe <sub>0.2</sub> ) [Fe <sub>1.6</sub> Zn <sub>0.4</sub> ] O <sub>3.90</sub>	18.1 (2.48)	0.20	8.422	2.04	1.93	122.8°	6.46	35.3	1440	57	250
RA52	(Zn <sub>0.6</sub> Fe <sub>0.4</sub> ) [Fe <sub>1.7</sub> Zn <sub>0.3</sub> ] O <sub>3.95</sub>	20.8 (3.09)	0.40	8.436	2.10	1.90	123.3°	4.24	40.4	500	27	100

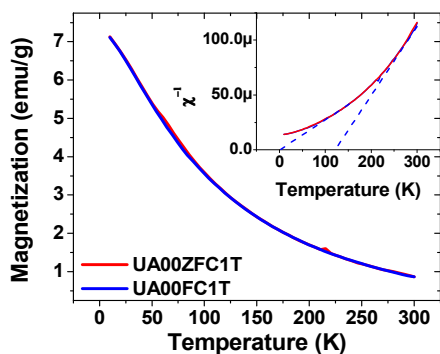
D( $\sigma$ ): Average crystallite size (standard deviation of crystallite size distribution); x: Degree of inversion; a: Lattice parameter; R (I, hkl): Goodness of fit; M<sub>s</sub>: Saturation magnetization; H<sub>c</sub>: coercivity; T<sub>B</sub>: Blocking temperature.

### 1 **Structure Refinement:**

2 Zinc ferrite has a cubic crystal structure, which belongs to the space group  $Fd\bar{3}m$  (JCPDS card no. 22-1012). For structure  
3 refinement, the atomic co-ordinates were taken from the initial report (ICSD Database No: 91827) and structure refined to  
4 completion. The GSAS package<sup>28</sup> was employed for Rietveld refinement. The profiles were fitted using a pseudo-Voigt  
5 function. A Chebyshev polynomial consisting of 10-16 coefficients was used to define the background. As iron and zinc are  
6 in special positions in zinc ferrite, only positional parameters of the oxygen atoms were refined. Further, the thermal  
7 parameters of the iron and zinc atoms were refined alternately with the occupancies. Details of crystallographic data and  
8 Rietveld difference plots are given in supplementary section S2, whereas the relevant crystal structure data are displayed in  
9 Table 1.

### 10 **Results and discussion:**

11 The as-prepared sample (UA00) was found to be ferrimagnetic at low temperatures (<30 K) and superparamagnetic at room  
12 temperature, characteristic of nano-sized ferrite particles.<sup>27</sup> But zinc ferrite in the bulk is known to be ferrimagnetic only  
13 below the Néel temperature ( $T_N=10$  K). Therefore, there must be a dominant exchange interaction other than  $J_{BB}$  present in  
14 the as-prepared sample which, in turn, indicates the possible presence of a certain degree of inversion in the ferrite lattice. To  
15 support this inference, temperature-dependent magnetization of UA00 was measured in an applied field of 1 T (Figure 1).  
16 Such a high field was chosen to ensure that the disordered spins present at the surface (if any) were quenched, thus enabling  
17 the identification of the contribution of superparamagnetism in the tiny crystallites of UA00. The ZFC and FC curves were  
18 found to overlap exactly everywhere, attesting to the complete quenching of the disordered spins.<sup>19</sup> The temperature-  
19 dependent inverse susceptibility plot (inset of Figure 1) reveals a slope in the temperature range 10 K to ~100 K that is  
20 different from the slope in the region 100 K to 300 K (as denoted by the dotted lines). Such behaviour is a signature of the  
21 presence of superparamagnetism during the transition from ferrimagnetism to paramagnetism. Thus, a definite but unknown  
22 degree of inversion in the as-prepared sample is evident.



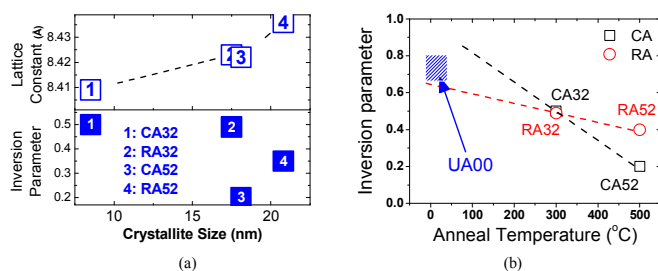
23

24 **Figure 1: Magnetic characterization of UA00 (as-prepared sample); M-T plots at a high field (1 T) and (in inset) Temperature-**  
25 **dependent inverse susceptibility plot.**

1 However, the saturation magnetization in the sample UA00, attributable to partial inversion, is not high (12.5 emu/g; Table  
 2 S1) even at a very low temperature (30 K). A previous report<sup>2</sup> suggests that, as the inversion parameter ( $x$ ) increases,  $M_s$   
 3 increases initially, but decreases for  $x > 0.65$ . Thus, the reason behind the measured low value of magnetization in UA00 could  
 4 either be a high degree of disorder among the surface spins due to nanocrystallinity, or an inversion parameter ( $x$ ) that is  
 5 considerably higher than 0.65, or both. Therefore, it is difficult to guess the extent of inversion from the results obtained by  
 6 magnetic characterizations alone. Other specialized tools, such as Rietveld refinement of high resolution PXRD data can be  
 7 useful for the accurate determination of ' $x$ '. But, the barely crystalline<sup>27</sup> nature of the UA00 samples does not permit useful  
 8 Rietveld analysis. On the other hand, the determination of ' $x$ ' for the well-crystallized annealed samples is possible but the  
 9 values are expected to differ from their un-annealed counterpart. However, effect of annealing on ' $x$ ' could lead us to a trend  
 10 that could allow us to estimate the extent of inversion induced in  $ZnFe_2O_4$  during synthesis. A way to control ' $x$ ' can also  
 11 emerge from that trend. Furthermore, the effect of annealing on other specific magnetic properties, such as interparticle  
 12 dipolar interactions can also be evaluated.

### 13 *Effect of annealing on inversion and magnetization*

14 The inversion parameters of the annealed  $ZnFe_2O_4$  samples were determined by Rietveld refinement of high-resolution XRD  
 15 data gathered at room temperature. The refined site occupancies and the fitting factors of all annealed samples are given in  
 16 Table 1, along with the unit cell parameters, bond angles, and ' $x$ '. It is to be noted that inversion indeed is present in all  
 17 samples and that the degree of inversion is much higher ( $\sim 0.5$  for both CA32 and RA32) than reported in the  
 18 literature<sup>6,29</sup> (typically in the order of 0.2). The distribution of cations over 'A'- and 'B'-sites of spinel lattice with various  
 19 degrees of inversion is schematically illustrated in Fig. S4 in supplementary section S4.

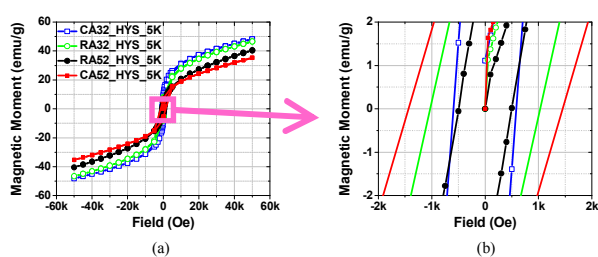


20

21 **Figure 2: (a) Inversion parameter and lattice constant of annealed samples, plotted against crystallite size; (b) Graphical**  
 22 **representation of the proposed value of inversion parameter in as-prepared samples [Note: the dashed lines are drawn merely to**  
 23 **guide the eye]**

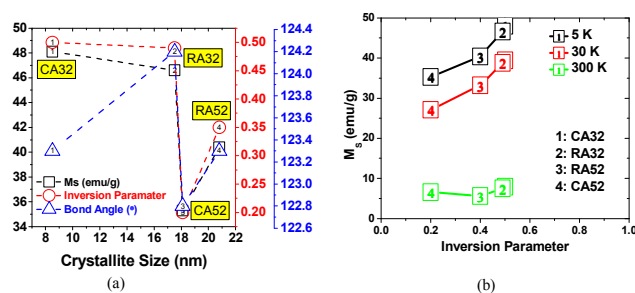
24 The impact of inversion on the characteristics of different samples will be different, as inversion invariably introduces strain  
 25 in the crystal system, which affects the lattice constant. The variation of the lattice constant (a) and ' $x$ ' with crystallite size is  
 26 plotted in Figure 2a. The lattice constant increases quite linearly with crystallite size, whereas the inversion parameter does  
 27 not follow any specific trend. However a trend can be observed if *the CA and RA samples are considered separately* (Figure  
 28 2b). The inversion parameter decreases from 0.5 to 0.2 for CA samples whereas, for RA samples, the change is from 0.49 to  
 29 0.40 with the increase in size as expected.<sup>30,29</sup> It is to be noted that the reduction in ' $x$ ' is markedly different for CA and RA  
 30 samples. Thus, the annealing protocol has great influence on the degree of inversion and not on annealing temperature alone.

1 In addition, the reduction in the inversion parameter happens to be correlated with increasing annealing temperature, as  
 2 observed in the previous reports.<sup>6</sup> Such dependence of the inversion on the annealing temperature, rather than on crystallite  
 3 size, can be explained by considering the heating mechanism (discussed in detail in the Section S3 of supplementary  
 4 information) in the RA and CA protocols. Due to the slow and prolonged heating and cooling in the CA protocol, displaced  
 5 cations “come back more completely” to their thermodynamically preferred locations ( $Zn^{2+}$  to A sites and  $Fe^{3+}$  to B sites). In  
 6 the RA protocol, the rapid heating and subsequent quenching barely support the migration of cations. Thus, the reduction in  
 7 ‘x’ in CA samples is much greater than in RA samples. It can therefore be concluded that the as-prepared sample (UA00)  
 8 must have an inversion parameter much greater than 0.5 and, keeping the low (12.5 emu/g at 30 K) value of  $M_S$  in mind, it is  
 9 surmised that the inversion parameter of the as-prepared sample is of the order of 0.75 or more, as depicted in Figure 2b.



10

11 **Figure 3: M-H in annealed samples measured at 5 K; (a) full-scale plot and (b) zoomed-in plot to determine  $H_C$**



12

13 **Figure 4: (a) Dependence of  $M_S$ , inversion parameter ( $x$ ) and the A-O-B bond angle on particle size; (b) Effect of inversion  
 14 parameter on  $M_S$  [Note: the dashed lines are drawn merely to guide the eye]**

15 The effect of inversion on saturation magnetization can be assessed by the measured hysteresis in the samples. Magnetization  
 16 versus applied field ( $M$  versus  $H$ ) measured at 5 K is therefore plotted for all the annealed samples in Figure 3a. As any  
 17 ferrimagnet would, the samples display hysteresis loops (Figure 3a and 3b). The saturation magnetization ( $M_S$ ) and the  
 18 coercivity ( $H_C$ ) measured at 5 K of all the annealed samples are tabulated in Table 1. It is to be noted that the annealed  
 19 samples display a much higher coercivity at 5 K than at 30 K or at room temperature.<sup>27</sup> The plausible reason for this is  
 20 discussed below.

21 We now consider the influence of the inversion parameter on the magnetization of partially inverted zinc ferrite.  
 22 Magnetization is found to be influenced strongly by the presence of inversion in the crystal structure of zinc ferrite.  
 23 Measurements made at 5 K and 30 K (Figure 4b) indeed demonstrate the enhancement of  $M_S$  due to an increasing degree of

inversion. A similar trend is visible even at room temperature (300 K), though not so prominently. It is also to be noted that the influence of the inversion parameter ( $x$ ) on  $M_S$  is very prominent near  $x = 0.5$ , i.e., a little change in inversion near the value 0.5 is enough to alter the saturation magnetization of these zinc ferrite samples. However, there is no specific trend observed to establish the dependence of  $M_S$  on crystallite size. Rather, as evident from Figure 4a, and as may be expected from the magnetic interactions made possible by partial inversion,  $M_S$  follows the degree of inversion closely. This observation illustrates that the processing of spinel nanoferrites has greater influence of on their magnetic properties than their crystallite size does.

The exchange interaction is also influenced by the bond angle (A-O-B) of the spinel structure. Usually, this angle is  $\sim 120^\circ$  in normal spinels, whereas the interaction is expected to reach its pinnacle when the angle is  $180^\circ$ . It is observed (as shown in Figure 4a) that the  $M_S$  also follows the bond angle closely except for the sample CA32, which possesses the highest  $M_S$  (50 emu/g at 5 K), even though the bond angle is relatively less obtuse.

### *Effect of annealing on surface disorder and coercivity:*

The temperature-dependent magnetization (M-T plot) of the annealed samples, measured under both ZFC (red) and FC (blue) conditions, is shown in Figure 5. The peaks of ZFC curves for all annealed samples are situated at greater than the Néel temperature (10 K for bulk zinc ferrite), suggesting that the materials are superparamagnetic.<sup>19</sup> The temperature corresponding to the peaks represents the blocking temperature ( $T_B$ ), where thermal energy balances magnetic energy. The  $T_B$  of each sample is the maximum in its normalized M-T plot obtained under ZFC conditions (Figure 6a and Table 1). The relationship between the crystallite size and  $T_B$  is shown in Figure 6b.

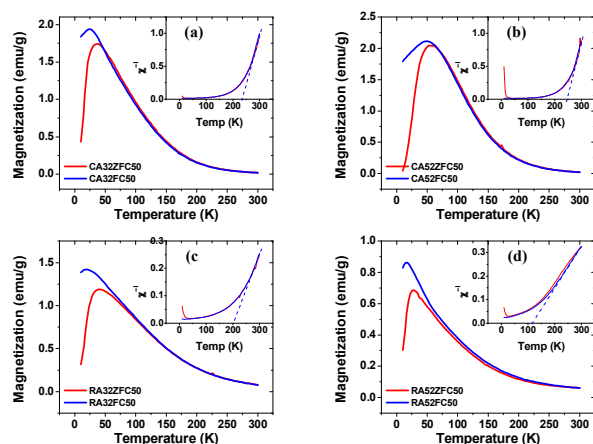
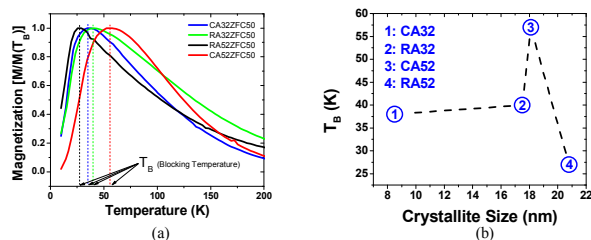


Figure 5: FC/ZFC plots of annealed samples: (a) CA32, (b) CA52, (c) RA32 and (d) RA52; measured at a low field (50 Oe), and (inset) the temperature-dependent inverse susceptibility



1

2 **Figure 6: (a) Normalized ZFC and (b) TB versus crystallite size; [the line in (b) is drawn merely as a guide to the eye]**

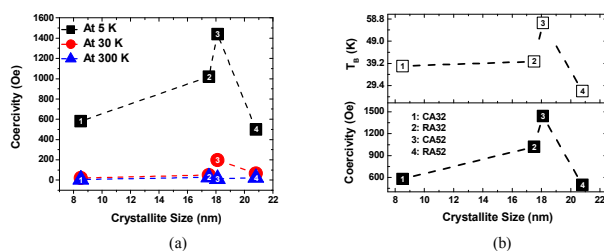
3 Before discussing the implications of different blocking temperatures of different samples, let us consider the traces of  
 4 superparamagnetism and the extent of surface disorder in the samples, if any. The plots of inverse susceptibility ( $\chi^{-1}$ ) versus  
 5 temperature (inset of Figure 5) reveal the gradual shift of slopes from the low temperature to high temperature, i.e., a gradual  
 6 transition from the superparamagnetic (SP) to the paramagnetic (P) regime, confirming the presence of superparamagnetism  
 7 in all the samples. It is to be noted that the mean crystallite size in three out of four samples is slightly larger than the  
 8 superparamagnetic critical size ( $\sim 17$  nm) – closely associated with the size beyond which any particle tends to become multi-  
 9 domain – beyond which superparamagnetism is no longer exhibited.<sup>29</sup>

10 The temperature at which the internal magnetic order starts breaking can be estimated from the slope of the curve in the P  
 11 regime, as marked by the dashed line for all the samples, and is tabulated as  $T_0$  in Table 1. It is found to be  $\sim 250$  K for the  
 12 conventionally annealed samples CA32 and CA52, while it is  $\sim 200$  K and 100 K for RA32 and RA52, respectively. This is  
 13 an interesting observation, indicating that the internal magnetic order breaks down at a much lower temperature in rapid-  
 14 annealed samples than in conventionally annealed samples. The plausible reason could be the weaker magnetic ordering in  
 15 them, i.e., the presence of a smaller magnetic moment and/or the presence of many more disordered surface spins. However,  
 16 the saturation magnetization of both RA32 and RA52 is much larger than in CA52. Therefore, there must be some other  
 17 factors that influence the early breaking of internal magnetic order in them. A closer look at the M-T is required to  
 18 understand this.

19 In the RA samples, unlike in the CA samples, the ZFC/FC curves (Figure 5) are separated at a temperature slightly above  $T_B$ .  
 20 Such magnetic behaviour is known<sup>20</sup> to mark the presence of a spin glass-like surface layer in which random exchange  
 21 interactions occur due to the existence of dangling bonds and the breaking of translational symmetry at the surface; such a  
 22 layer could extend to a few atomic layers beneath the sample surface. The separation of the ZFC and FC curves is more  
 23 pronounced in RA52, which also has a smaller inversion parameter (than RA32), and thus weaker magnetic ordering. This  
 24 causes RA52 to become paramagnetic at a much lower temperature than the other annealed samples and to display the lowest  
 25 measured value of  $T_B$  (25 K) among the annealed samples.

26 The effect of process-induced surface disorder and their subsequent influence on inter-particle interaction is clearly visible in  
 27 the trend in the measured coercivity. The coercivity of the annealed samples, measured at different temperatures, is plotted  
 28 against the crystallite size in Figure 7a. Coercivity is found to increase initially up to a certain size ( $\sim 18$  nm) and then to  
 29 decrease. Such behavior has been reported earlier, and explained by the theory of transformation from a single domain to a  
 30 multi-domain structure.<sup>29</sup> However, the sample RA52 is found to be single domain in nature.<sup>27</sup> In addition to this, in the

1 present work, coercivity is found to follow  $T_B$  closely (Figure 7b). Therefore, the observed coercivity in these samples may  
 2 be understood as follows:



3  
 4 **Figure 7: (a) Particle size-dependence of coercivity in annealed samples; and (b) Effect of blocking temperature ( $T_B$ ) on coercivity**  
 5 **[Note: the dashed lines are drawn merely to guide the eye]**

6 CA52 is well-equilibrated at 500 °C, resulting in rather large single-crystalline grains (~20 nm on the average) and a  
 7 significant reduction in ‘x’, and thus has a lower  $M_S$  than CA32. However, strong dipolar interactions between crystallites<sup>24</sup>  
 8 can be observed as individual particles have, on the average, a large magnetic moment due to their size and sufficiently high  
 9  $M_S$ . In contrast, sample RA32, with a similar particle size and even higher  $M_S$ , could only show coercivity that is much lower  
 10 than in CA52. This observation can be attributed to the strong screening of the interparticle dipolar interaction due to the  
 11 presence of a very high degree of surface disorder (as evidenced by the “split” in the FC-ZFC plot in Figure 5d), induced by  
 12 the rapid thermal annealing process. A similar screening effect has been observed in cobalt and manganese ferrite  
 13 nanoparticles in silica matrix<sup>30</sup> as well as in  $Fe_3O_4$  and  $\gamma-Fe_2O_3$  nanoparticles.<sup>31</sup> RA32 is also a rapid-annealed sample and has  
 14 surface disorder but less than that in RA52 (Figure 5c). It also has a high  $M_S$ . As a result, the screening effect is too low to  
 15 overwhelm the dipolar interaction and thus RA32 exhibits coercivity larger than does RA52, but smaller than CA52. Finally,  
 16 in sample CA32, the absence of surface disorder and a very high value of  $M_S$  together do not result in a strong interparticle  
 17 dipolar interaction simply because of the lack of a sufficiently large magnetic moment in its tiny crystallites (~8 nm).  
 18 Therefore, the dipolar interaction certainly depends on the crystallite size as well as on the presence of surface disorder that  
 19 can be controlled by the processing technique employed.

## 20 Conclusions

21 In summary, Rietveld analysis confirms that a high degree (~0.50) of inversion is achieved in zinc ferrite nanocrystallites.  
 22 Analysis of crystal data of various annealed samples indicates that inversion parameter as high as 0.75 could be induced in  
 23  $ZnFe_2O_4$  by microwave-assisted solvothermal synthesis at a very low temperature (<100°C), due to the rapid nature of the  
 24 process. The degree of inversion then can be “tuned-down” to a desired level by annealing at an appropriate temperature  
 25 through an appropriate protocol. Rapid annealing is found to arrest the degree of inversion efficiently at a value higher than  
 26 conventional slow annealing. In addition, rapid annealing is an effective tool to control the surface disorder in  
 27 nanocrystallites, which can screen the interparticle dipolar interaction and thus coercivity. Coercivity of the samples tracks  
 28 the blocking temperature closely, reaching 1440 Oe (at 5 K) in the sample with the highest  $T_B$ . On the other hand, saturation  
 29 magnetization follows the degree of inversion and not the crystallite size. These findings demonstrate that key magnetic  
 30 properties, along with the surface disorder of nanocrystalline zinc ferrite, can be tailored not only by adjusting crystallite size,

1 but also through judicious post-synthesis annealing protocols, apart from the temperature and duration of annealing. Such an  
2 approach promises an alternative and versatile way to tune inversion and surface disorder for the development of various  
3 magnetic nanomaterials with different structures for different futuristic applications as well as for further studies on the  
4 process of magnetization in spinel ferrimagnets.

## 5 **Acknowledgements**

6 The authors are grateful for financial support from the Dept. of Information Technology, Govt. of India and from the  
7 National Program on Micro and Smart Systems (NPMASS).

## 1 References

- 2 1. S. Stewart, S. Figueroa, J. Ramallo López, S. Marchetti, J. Bengoa, R. Prado, and F. Requejo, *Phys. Rev. B*, 2007, **75**,  
3 3–6.
- 4 2. R. Valenzuela, *Phys. Res. Int.*, 2012, **2012**, 1–9.
- 5 3. S. L. Darshane, R. G. Deshmukh, S. S. Suryavanshi, and I. S. Mulla, *J. Am. Ceram. Soc.*, 2008, **91**, 2724–2726.
- 6 4. M. A. Hakim, M. Manjurul Haque, M. Huq, and P. Nordblad, *Phys. B Condens. Matter*, 2011, **406**, 48–51.
- 7 5. R. Sai, K. J. Vinoy, N. Bhat, and S. A. Shivashankar, *IEEE Trans. Magn.*, 2013, **49**, 4323–4326.
- 8 6. S. Oliver, H. Hamdeh, and J. Ho, *Phys. Rev. B*, 1999, **60**, 3400–3405.
- 9 7. C. Bárcena, A. K. Sra, G. S. Chaubey, C. Khemtong, J. P. Liu, and J. Gao, *Chem. Commun. (Camb.)*, 2008, **3**, 2224–  
10 6.
- 11 8. F. Li, H. Wang, L. Wang, and J. Wang, *J. Magn. Magn. Mater.*, 2007, **309**, 295–299.
- 12 9. R. Dom, G. S. Kumar, N. Y. Hebalkar, S. V. Joshi, and P. H. Borse, *RSC Adv.*, 2013, **3**, 15217.
- 13 10. D. Venkateshvaran, M. Althammer, A. Nielsen, S. Geprägs, M. Ramachandra Rao, S. Goennenwein, M. Opel, and R.  
14 Gross, *Phys. Rev. B*, 2009, **79**, 134405.
- 15 11. Y. Yafet and C. Kittel, *Phys. Rev.*, 1952, **87**, 290–294.
- 16 12. G. Samara and A. Giardini, *Phys. Rev.*, 1969, **186**, 577–580.
- 17 13. R. Weisz, *Phys. Rev.*, 1951, **84**, 379–379.
- 18 14. D. Carta, M. F. Casula, P. Floris, A. Falqui, G. Mountjoy, A. Boni, C. Sangregorio, and A. Corrias, *Phys. Chem.*  
19 *Chem. Phys.*, 2010, **12**, 5074–83.
- 20 15. J.-M. Li, X.-L. Zeng, and Z.-A. Xu, *Appl. Phys. Lett.*, 2013, **103**, 232410.
- 21 16. Y. Xu, Y. Liang, L. Jiang, H. Wu, H. Zhao, and D. Xue, *J. Nanomater.*, 2011, **2011**, 1–5.
- 22 17. O. M. Lemine, M. Bououdina, M. Sajieddine, A. M. Al-Saie, M. Shafi, A. Khatab, M. Al-hilali, and M. Henini, *Phys.*  
23 *B Condens. Matter*, 2011, **406**, 1989–1994.

- 1 18. H. Ehrhardt, S. J. Campbell, and M. Hofmann, *Scr. Mater.*, 2003, **48**, 1141–1146.
- 2 19. C. Upadhyay, H. Verma, V. Sathe, and A. Pimpale, *J. Magn. Magn. Mater.*, 2007, **312**, 271–279.
- 3 20. R. D. K. Misra, S. Gubbala, A. Kale, and W. F. Egelhoff, *Mater. Sci. Eng. B*, 2004, **111**, 164–174.
- 4 21. L. Hao, Y. Zhao, Q. Jiao, and P. Chen, *RSC Adv.*, 2014, **4**, 15650.
- 5 22. M. J. Akhtar, M. Nadeem, S. Javaid, and M. Atif, *J. Phys. Condens. Matter*, 2009, **21**, 405303.
- 6 23. J. Lee, *J. Alloys Compd.*, 2001, **325**, 276–280.
- 7 24. V. Blanco-Gutierrez, R. Saez-Puche, and M. J. Torralvo-Fernandez, *J. Mater. Chem.*, 2012, **22**, 2992.
- 8 25. S. Komarneni, M. C. D. Arrigo, C. Leonelli, and G. C. Pellacani, *J. Am. Ceram. Soc.*, 1998, **81**, 3041–3043.
- 9 26. R. Pązik, E. Piasecka, M. Małicka, V. G. Kessler, B. Idzikowski, Z. Śniadecki, and R. J. Wiglusz, *RSC Adv.*, 2013, **3**,  
10 12230.
- 11 27. R. Sai, S. D. Kulkarni, K. J. Vinoy, N. Bhat, and S. A. Shivashankar, *J. Mater. Chem.*, 2012, **22**, 2149.
- 12 28. A. C. Larson and R. B. Von Dreele, *General Structure Analysis System (GSAS)*, Los Alamos National Laboratory  
13 *Report LAUR*, 2004, vol. 748.
- 14 29. V. Blanco-Gutierrez, E. Climent-Pascual, M. J. Torralvo-Fernandez, R. Saez-Puche, and M. T. Fernandez-Diaz, *J.*  
15 *Solid State Chem.*, 2011, **184**, 1608–1613.
- 16 30. V. Blanco-Gutiérrez, M. J. Torralvo-Fernández, and R. Sáez-Puche, *J. Phys. Chem. C*, 2010, **114**, 1789–1795.
- 17 31. M. I. Dar and S. A. Shivashankar, *RSC Adv.*, 2014, **4**, 4105.

18